Investigation of the Effectiveness and Robustness of an MEMS-Based Structural Health Monitoring System for Composite Laminates

Francesco Caimmi, Stefano Mariani, Marco De Fazio, and Paolo Bendiscioli

I. Introduction

HEALTH monitoring of real-life structures (especially the safety-critical ones, see [1]) is nowadays perceived as a critical and important field of study. Health monitoring systems have to provide timely information along the whole life cycle of the structures [2], [3], to prevent failures under service or extreme external actions. To work properly, the systems require a reliable model of the structure to be continuously fed by the information collected by permanently installed sensors.

Focusing on composite laminates, consisting of a stacking sequence of laminae or plies joined together through resin enriched regions, structural health monitoring plays a prominent role. In fact, composite structures are now adopted in various fields ranging from aeronautics to civil engineering; in all the cases, the high stiffness to weight and strength to weight ratios featured by composite materials, specifically designed in order to attain them, are appropriately exploited to guarantee higher performances. This can also increase the sensitivity of the structural components to defects, in case their toughness is not high enough to guarantee an overall ductile response, providing a possible nucleation of catastrophic failure events.

The microstructure of composites, characterized by interfaces (or interphases) between materials featuring different mechanical and thermal properties [4]–[6], raises issues linked to the health monitoring. As the mentioned interfaces, prone to fail by cracking under repeated external actions [7]–[9], are buried inside the structure, an accurate, effective and fast on-line monitoring strategy has to be devised.

In case of composite structures interacting with harsh environments or asked to feature specific aerodynamic properties, an attractive approach for their continuous monitoring is to embed the sensors inside the bulk of the structure (material-integration) during the production process, taking advantage of the interlaminar regions between laminae. This strategy was followed, e.g. in [10]–[14], to install sensing systems constituted by fiber Bragg grating, piezoelectric sensors, high resistivity electric grids, or photonic crystal fibers. All these methods can attain high accuracy in detecting delamination, i.e. interlaminar debonding between adjacent laminae, but they also cause a distortion of the microstructure [15]–[17]. Such distortion can be hardly controlled in small composite panels, may get increased in real-life structures by the structural dimensions, and it finally leads to the nucleation of small defects in the resin-enriched regions surrounding the sensors. This nucleation of defects is usually triggered also by the induced local stress concentration [18]. The final outcome of this embedding approach might be as summarized in [19], where piezoelectric sensors were adopted in the monitoring system: laminates failed by cracking exactly where the sensors had been placed, with a remarkable reduction of the overall strength and toughness of the composite.

Manuscript received February 17, 2014; accepted March 25, 2014. Date of publication April 4, 2014; date of current version May 22, 2014. This work was supported by STMicroelectronics through the Material Reliability Project. The associate editor coordinating the review of this paper and approving it for publication was Dr. Dirk Lehmhus.

F. Caimmi is with the Department of Chemistry, Materials and Chemical Engineering, Politecnico di Milano, Milan I-20133, Italy (e-mail: francesco.caimmi@polimi.it).

S. Mariani is with the Department of Civil and Environmental Engineering, Politecnico di Milano, Milan I-20133, Italy (e-mail: stefano.mariani@polimi.it).

M. De Fazio is with the Advanced System Technology, STMicroelectronics, Agrate Brianza I-20041, Italy (e-mail: marco.de-fazio@st.com).

P. Bendiscioli is with the AMS Group, STMicroelectronics, Cornaredo I-20010, Italy (e-mail: paolo.bendiscioli@st.com).

Color versions of one or more of the figures in this paper are available online.

Another important issue linked to this monitoring scheme, is related to its reliability, and specifically to the capability to transfer the local strain field from the composite to the sensors [11], [16], [20]. Overall, it is recognized that, if not accurately designed, deployed and embedded, this class of monitoring systems may have adverse effects on the life cycle of the structure.

In [21], partially moving from the results gathered in [22], we proposed a surface-mounted monitoring scheme, adopting micro electro-mechanical system (MEMS) accelerometers as sensing devices. Dealing with light weight composite structures, the adoption of non-invasive MEMS sensors, extremely light in weight on their own, appears to be of paramount importance. Likewise the previously listed strategies, this on-line, continuous monitoring of the structural health does not directly track the presence and size of the delaminated area(s); instead, collected data have to be post-processed to indirectly estimate the health of the structure. We proposed to adopt commercial-off-the-shelf sensors, developed for mobile and gaming applications, hence characterized by a huge mass production and extremely low costs. Obviously, such sensors cannot feature the same accuracy of the previously listed sensing devices, and require ad-hoc post-processing steps in order to get informative data on the health of the laminates.

In [21], we shaped the problem frame and run an experimental campaign to collect results relevant to a so-called mode I (opening only) propagation of the delaminated area, supposed to be the only structural damage. Through a simple, beam bending model of the tested specimens, the experimental and theoretical outcomes were found to be in fairly good agreement, provided that the analysis is moved to the frequency domain. In this work, we discuss a different data reduction procedure for the same kind of mode I testing, handling a different composite material. We therefore extend the former investigation, showing for the methodology results related to its effectiveness (in terms of sensitivity to damage) and robustness (in terms of repeatability of the monitored state at varying specimen). Moreover, we show that experimental and theoretical results (the latter ones still guided by beam bending models) do agree well, independently of the local stress state at the tip of delamination; hence, also so-called mode II (shearing only) conditions are accounted for and explored. This aspect looks interesting too, as the microstructure (both at the lamina and panel levels) may lead to different composite behaviors in case of mode I or mode II loading conditions.

The remainder of this paper is organized as follows. In Section II details relevant to the composite material, the laminate production and the loading protocols are provided; moreover, features of the adopted MEMS accelerometer are given, together with details on how it has been mounted, through its board, on the surface of the tested specimens. Section III deals with the theoretical, beam bending model of the composite response to different loadings, to provide the engine for the monitoring of the structural health, i.e. of the delamination length. In Section IV the experimental data are interpreted on the basis of the previously discussed theoretical model, showing a good accuracy as far as the sensed structural effects of the delamination length are concerned. Finally, in Section V some concluding remarks on this investigation are provided, along with proposals to improve the current results.

II. Experimental

To extend the experimental campaign reported by Mariani et. al in [21], in this work two different kinds of laboratory test configuration have been considered: the double-cantilever-beam (DCB) [23] one, and the end-loaded-split (ELS) [24] one. Schematics (with notation) and pictures of the deformed shape of the specimens under the two different loading conditions are given in Figure 1. Both the setups have been adopted to test very simple and slender (beam like) composite samples with constant rectangular cross section, containing a delamination that was artificially inserted on the laminate midplane during manufacturing. DCB specimens are subject to point loads inducing an opening of the delamination (mode I), while ELS specimens are loaded in a cantilever fashion to induce shearing (mode II) of the delaminated arms.

The same laminated sample geometry has been considered for both DCB and ELS configurations, using a carbon/fibre reinforced epoxy, supplied as pre-pregs. The reinforcement consisted of a 8 harness satin fabric made of Hexcel™HexTow™AS4C fibers; the matrix was a toughened epoxy resin (HexPly™8552). Composite panels were prepared by manual lay up using a $[0]_{12}$ ply stacking sequence, see e.g. [25] and [26], cured in autoclave and milled to the final dimensions using a diamond saw and a mill. To nucleate the initial delamination, a 13 μm thick PTFE film was placed on the laminate midplane. Overall sample dimensions were $200 \times 25 \times 4.5$ mm (length, width, thickness), while the initial delamination length was 60 mm. These dimensions are compliant with the ASTM D-5528 standard for interlaminar fracture testing of composite materials [23]. In order to connect the samples to the testing machine, aluminum load blocks have been bonded to the specimen ends with an epoxy adhesive (3M DP-490); these blocks have been then connected to the test rig using pins. For the two test setups, the geometry and dimensions of the samples and of the load blocks are provided in Figure 2.

The specimens were instrumented with the commercial-off-the-shelf LIS3LV02DQ three-axis, digital output MEMS accelerometer [27]. This sensor is characterized by a full scale of $\pm 2g$ (which can be switched to $\pm 6g$, g being the gravity acceleration), a bandwidth of 640 Hz, a sensitivity of about 1000 LSb/g (LSb standing for least significant bit) and a resolution of 1 mg. This sensor senses also the gravity acceleration, so the output along the y-axis (see Figure 1) is expected to be $-1g$ when the specimens are unloaded. In a quasi-static framework, this feature can be exploited to get insights into the specimen deformation through local inclinations relative to the gravity direction.

As the purpose of the present investigation is the assessment of the sensor's capabilities, the instrumentation has been devised in a simple way, by using the evaluation board typically supplied by STMicroelectronics. This board carries the accelerometer, a microprocessor for data acquisition and an USB connector for power supply and communication.

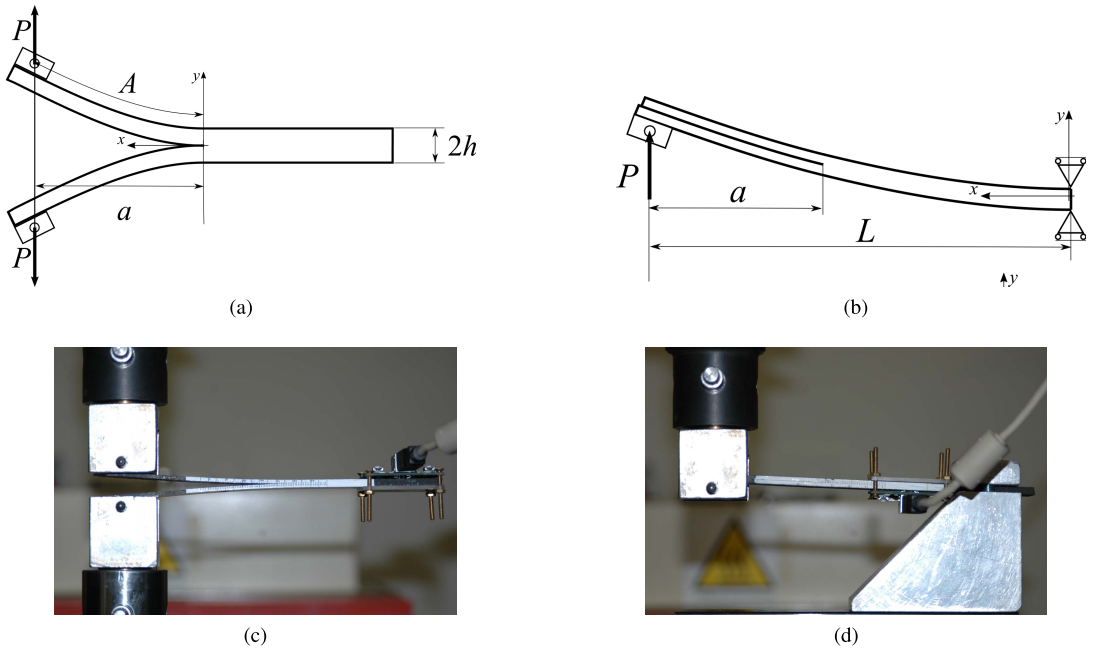

Fig. 1. Schemes (top row) and pictures (bottom row) of the test setups: (a)–(c) DCB test and (b)–(d) ELS test.

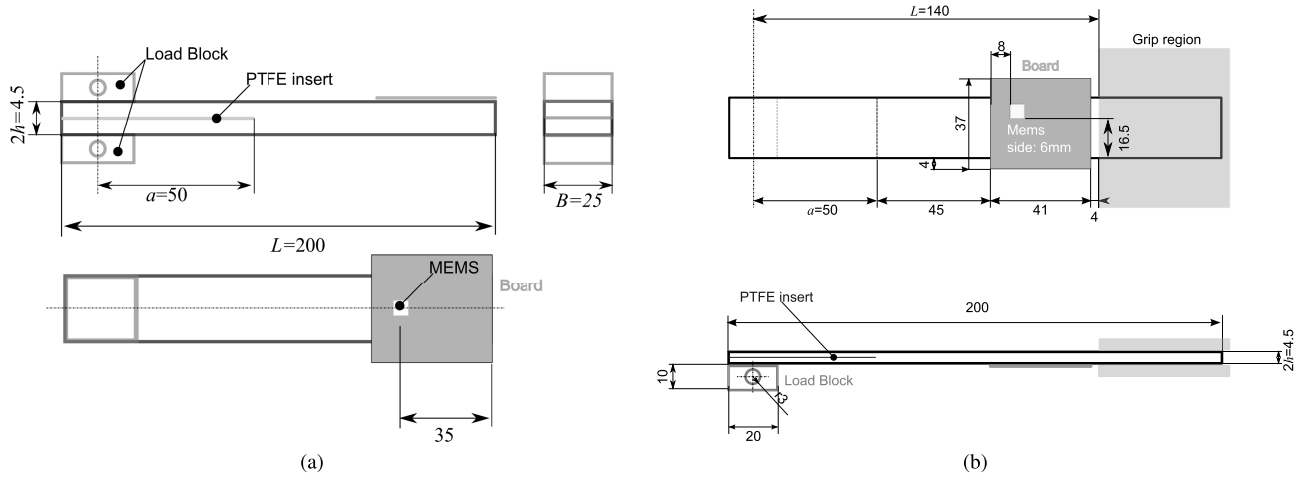

Fig. 2. Dimensions (in mm) of the samples and board position: (a) DCB and (b) ELS.

The positioning of the board over the specimens, in the two tested configuration, is shown in Figure 2. The board has been rigidly joined to the specimen by using four screws and a back plate. The back plate was made of PMMA, to result flexible enough and follow the specimen deformation without breaking.

The use of the board has allowed not to design a flexible circuit board to connect the chosen accelerometer to the specimen surface. On the other hand, the use of such a board, whose dimensions are much larger than those of the MEMS sensor (see Figure 2), has provided some constraints on the board and sensor placement. For the ELS configuration, it has also posed limits on the displacements that can be prescribed, so as to be withstood by the board itself too. Anyhow, with the present setup it has been possible to attain displacements causing a crack propagation of about 25 mm, which was considered adequate for the purpose of this study.

By placing the board as shown in Figures 1 and 2, the delamination growth has been monitored using a time-continuous protocol for the longest possible time span. A possible drawback of such a positioning is that it corresponds to the region featuring the smallest accelerations along the specimen axis. Furthermore, it should be noted that the relatively low precision of sensor positioning can add some scattering to the measurements (see relevant comments in Section IV).

The mechanical tests were performed on an Instron 1185R5800 electro-mechanical testing machine, equipped with a 10 kN load cell. Due to the specific loading rigs used, the upper load point of the DCB specimen is actually fixed, i.e. it cannot move in any direction, and the load point of the ELS specimen is fixed too.

The testing protocol adopted for both the setups has been as follows: on each specimen, a series of different tests have

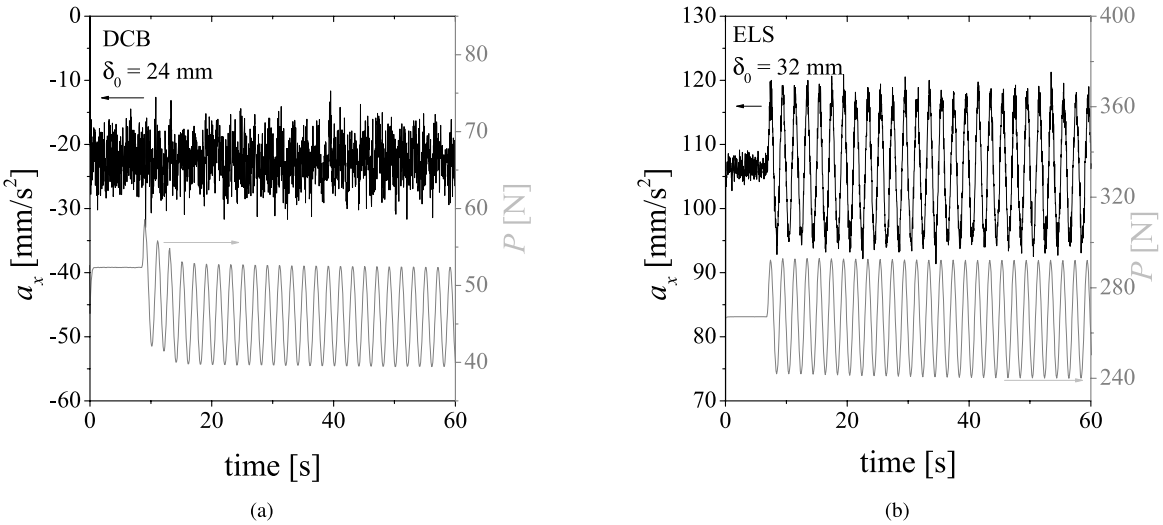

Fig. 3. Typical raw output (acceleration and load) for the two test configurations, along a single load step: (a) DCB and (b) ELS.

been run by prescribing a sinusoidal variation of the load point displacement δ, according to the following law

$$\delta = \delta_0 + \Delta\delta \sin(2\pi f_\delta t) \tag{1}$$

where δ_0 is the baseline displacement, $\Delta\delta$ is the amplitude of the displacement oscillation, t is time and f_δ is the test frequency. f_δ and $\Delta\delta$ have been respectively set to 0.5 Hz and 2.5 mm for all the tests; the baseline displacement δ_0 has been instead progressively increased from test to test on the same sample (or from one load step to the next one), so as to cause a stable delamination propagation. Moreover, δ_0 has been chosen to vary in a range of values so that crack propagation was confined at the beginning of each load step (see also [21]), according to the $\Delta\delta$ value adopted. The duration of each load step has been set to 200 cycles.

During each load step, the delamination length has been monitored by direct, optical observation of the specimens; to make such a measurement easier, the specimen sides have been coated with a thin layer of typewriter correction fluid and marks have been placed regularly along the specimens length as per [23]. Further details on the test protocol can be found in [21] and [28].

Typical results, in terms of load vs. time and acceleration vs. time traces as recorded during a single load step, are shown in Figure 3a and Figure 3b for the DCB and ELS configurations, respectively. The acceleration shown, a_x, is the component along the longitudinal x-axis, see Figure 1. Similar results have been obtained for the through-thickness, y-axis acceleration, and are not reported here for brevity.

For both configurations, the graphs show that the initial baselines for the measured accelerations are different from zero. As for the DCB specimen, this is due to the weight of the sample and of the sensing system, which slightly tilts the specimen axis. As for the ELS specimen, it is instead due to the fact that at $t = 0$ the sample is already under load, and an angle is formed between the gravity direction and the normal to the beam profile. As it can be seen, the acceleration output is rather noisy, in particular for the DCB case where the baseline signal is closer to zero. This noise requires the signal to be appropriately post-processed, as discussed in what follows.

As far as the load time histories are concerned, Figure 3 shows that, after initial drops during the first few cycles, the load peaks get constant and delamination no longer grows: a steady-state specimen configuration is therefore approached.

III. Crack Length Monitoring Schemes

For the two test configurations described before, different monitoring schemes for the delamination length have been developed, taking into account the relevant specimen responses and loading conditions at the crack tip. Mechanical models of the specimens have been therefore built in order to find a simple correlation between the crack length and the accelerations measured by the MEMS sensor.

As for the DCB specimen, a monitoring scheme derived using simple beam theory and exploiting the acceleration along the vertical (y) axis was developed and used by the present authors in [21]. Here we test a different scheme, exploiting instead the acceleration along the horizontal (x) direction.

The DCB specimen basically consists of two built-in cantilevers joined at the delamination tip (hence the name); this is of course a simplification of the actual behavior of the specimen, which does not take into account the very high stress gradients close to the delamination tip. The rest of the specimen ($x < 0$, see Figure 1a) can be considered approximately unloaded, so that it undergoes only rigid body motions. In the preceding discussion, distributed loads linked to the sample weight have been disregarded; this does not represent an issue, due to the light weight feature of composite materials.

Let $v(x)$ be the vertical displacement of the longitudinal axis of the DCB specimen. Within the framework of Bernoulli-Euler beam theory, which neglects shear deformations (see, e.g. [5]), and in case of small displacements, for a uniform rectangular cross section the solution of the beam equation with boundary conditions $v(a) = 0$ (fixed load point)

and $\mathrm{d}v(0)/\mathrm{d}x = 0$ (beam perfectly built-in at the delamination tip) yields

$$v(x) = \frac{4P\left(x^3 - a^3\right)}{EBh^3} \tag{2}$$

where P is the applied load, a is the delamination length, B is the out-of-plane sample width (see Figure 2a) and h is its thickness, E is the elastic modulus of the material along the x-axis (we recall that composite materials are anisotropic due to their microstructures, but once the stacking sequence has been defined the Young's modulus E of the whole laminate can be obtained). In (2), only the upper arm is considered; due to symmetry in the specimen geometry and loading conditions (see Figure 1a), the load point displacement δ results to be $2v(0)$. As stated in Section II, for the DCB test the upper load grip does not move, whereas the lower one is vertically, downward displaced by δ. The compliance of the specimen is thus given by

$$C(a) = \frac{\delta(a)}{P} \tag{3}$$

which of course depends on the delamination length a. As beam kinematics is characterized by cross sections keeping a plane shape when deformed, the longitudinal displacement field u can be expressed as

$$u(x, y) = u_{\mathrm{a}}(x) - y\frac{\mathrm{d}v}{\mathrm{d}x} \tag{4}$$

where $u_{\mathrm{a}}(x)$ is the axial displacement satisfying the differential equilibrium equation:

$$\frac{\mathrm{d}}{\mathrm{d}x}(E\mathcal{A}\frac{\mathrm{d}u_{\mathrm{a}}}{\mathrm{d}x}) = -\eta. \tag{5}$$

In (5), $\mathcal{A}$ is the cross section area of each arm of the laminate and η is the distribution of external axial forces acting on the beam. Since there is no net force acting along the x-axis and because of the zero displacement at the load point ($x = a$), the function u_{a} vanishes everywhere. Relations (2) and (4) thus provide the horizontal displacement field u, which is only due to the beam deflection and varies according to the following expression

$$u(x, y) = -\frac{12Px^2y}{EBh^3} \tag{6}$$

which fulfills the null condition at $x = 0$. For $x < 0$, the sample region where the sensor is placed, there is no net internal action so that the displacements of that part of the beam are the same as those at $x = 0$. Hence, according to the linear theory here considered, there should be no horizontal accelerations measured by the MEMS sensor.

However, since the thickness and, therefore, the bending stiffness of the specimen is rather small, the out-of-plane displacements can get large during loading, especially for large values of δ_0 in (1). Bending, even in the absence of any axial force η, can cause an axial displacement u_{a}, linked to the projection onto the horizontal axis x of the deformed geometry of the specimen arms, which is supposed to decrease at increasing load point displacement (see Figure 1a). Such non-zero axial displacement turns out to be a rigid body-like motion of the part of the specimen not bent by the opening load P, or by the relevant load point displacement δ. Hence, the difference between the actual length of the beam arms (A in Figure 1a) and the distance between the delamination tip and the load line a, which is of course zero in the undeformed configuration, may provide a way to determine the horizontal displacement of the undamaged part of the specimen. Unfortunately a closed form solution for the non-linear DCB problem featuring finite deformations, does not exist; in a work by Williams [29] an implicit solution was found, which cannot be adopted here for monitoring purposes. In the absence of such explicit theoretical interpretation of the data, as a monitoring engine we introduce an empirical correlation between the delamination length and the acceleration or better, as it is going to be discussed in Section IV, its Fourier transform.

Moving now to the ELS specimen, and consistently with the optimization procedure proposed by the authors in [30] and [31] to deploy MEMS sensors over complex structures, the quantity chosen for monitoring the delamination length is the rotation of the sample along its longitudinal axis. In fact, as the MEMS accelerometer is able to sense also the gravity acceleration, the output in terms of sensed acceleration components can be exploited to obtain the current orientation of the device relative to the vertical direction.

Consider now the reference system in Figure 1b. In this case, as long as the analysis is once again confined to the hypotheses outlined above and the delaminated arms can be considered perfectly built-in at the crack tip, the vertical displacement field in the undamaged region $x < L - a$ is straightforwardly obtained by integration of the beam equation as

$$v(x) = \frac{P(3L - x)x^2}{4EBh^3} \tag{7}$$

and does not depend on a. As we are interested in the region where the sensor is placed, there is no need to evaluate the displacements in the delaminated region; for the purpose of the present work, it will suffice to recall that the compliance of the ELS specimen is given by [29]:

$$C(a) = \frac{\left(a^3 + L^3\right)P}{2EBh^3} \tag{8}$$

Within the present beam theory, the in-plane rotation of the ELS specimen axis for $x < L - a$ can be obtained as $\phi(x) = \frac{\mathrm{d}v}{\mathrm{d}x}$. Dividing such rotation by the applied displacement δ and using (3) and (8), the following equality is recovered

$$\frac{\phi(x)}{\delta} = \frac{3(2L - x)x}{2\left(3a^3 + L^3\right)} \tag{9}$$

If x_{MEMS} stands for the position of the MEMS in the adopted reference frame, the aforementioned orientation of the sensor relative to the vertical direction can be easily evaluated, in the present quasi-static setting, as

$$\phi(x_{MEMS}) = \arctan\left(\frac{a_y}{a_x}\right) \tag{10}$$

IV. Results

Let us start by considering the DCB specimen. From the raw data collected in Figure 3a, it is rather evident that the time

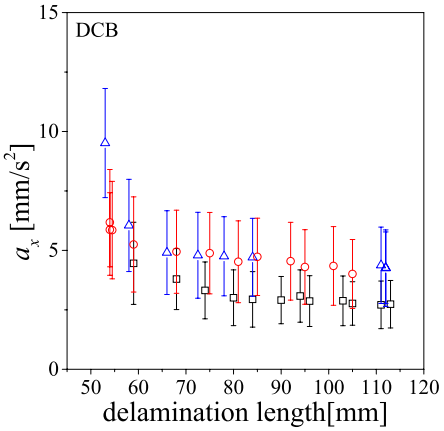

Fig. 4. DCB test: statistics of the sensed acceleration peaks at varying delamination length (different symbols correspond to different samples).

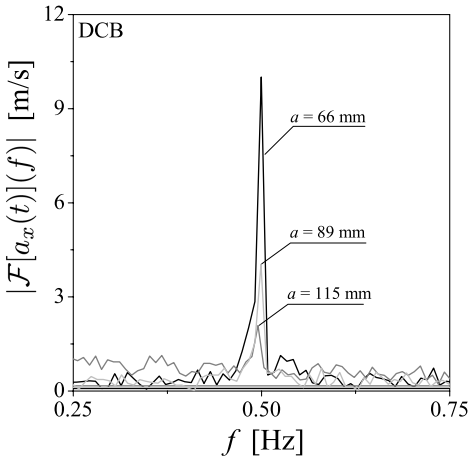

Fig. 5. DCB test: Fourier transform of the acceleration signals, as obtained while testing a single sample during three subsequent load steps.

history of the measured acceleration could be hardly used to infer the delamination length. Due to the high noise to signal ratio, there is no significant difference between the MEMS output before and during loading (which, for the case under consideration, starts varying sinusoidally around $t = 9$ s). Note that the same holds true also when considering the acceleration along the y-axis, see [21].

Figure 4 gathers the average values of the acceleration peaks and the relevant scattering, as recorded during each load step, reported against the corresponding delamination length. Here, different symbols have been adopted for different samples. In this plot, the delamination length a has been computed by measuring the specimen compliance C as the slope of the load vs. load point displacement curve, once the length got stationary after the initial transient stage mentioned in Section II, and then solving (3) for a. Due to the scattering in the data, there is no evidence for any correlation between the sensed acceleration peaks and the damage size. If a sensing scheme based on raw accelerations were employed, it would therefore be impossible to detect delamination growth. Although part of the scatter can be attributed to the positioning of the sensor board over the specimen, some sort of filtering technique can be adopted in order to get meaningful data. As proposed in [21], a Fourier transform has then been applied to the acceleration data; as an example, Figure 5 shows the results in the proximity of the prescribed displacement frequency $f_\delta = 0.5$ Hz. Plots referring to three different load steps are shown, at increasing baseline displacement δ_0 and, therefore, delamination length. It clearly emerges that peaks at the test frequency f_δ are well defined and sharp, and can be distinguished from the noise even for delamination lengths close to the maximum attainable with the proposed setup.

As reported in [21], Figure 5 shows that the peak amplitude decreases at increasing delamination length a; this feature can hence be adopted to establish a one-to-one relation between a and the sensor output. Relevant results, in terms of amplitude of the peak at f_δ against crack length are shown in Figure 6, where once again different symbols in the scattered data correspond to different samples. Although the scatter seems to keep growing for big delamination lengths, a clear correlation

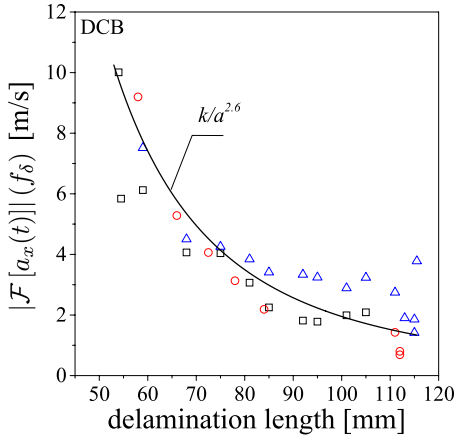

Fig. 6. DCB test: magnitude of the peak of Fourier transform of the acceleration signals at the test frequency $f_\delta = 0.5$ Hz, and best fitting according to the functional form provided by beam theory (different symbols correspond to different samples).

between the peak of the signal at the test frequency and crack length can be seen; the trend shown is rather similar to the one found in [21] on the basis of the beam bending theory described in Section III. The current data have been fitted in Figure 6 with a power law, k/a^n, where k and n are constants to be empirically tuned, as this functional form is the one expected in accordance with our previous works. The best fit of all the data, which is shown as a continuous line in Figure 6, yields $n = 2.6$, which is rather close to the theoretical value $n = 3$, see [21]. Even if empirical, such a correlation shows that MEMS sensors can be successfully adopted for monitoring the state (or health) of the composite laminate, even when small acceleration peaks have to be distinguished from the noise through the simple filtering technique here discussed.

As far as the ELS specimens are concerned, Figure 3b have reported that the sensed acceleration suffers from a noise level much reduced in comparison with the DCB case. A prognosis of the laminate health therefore turns out to be much easier. As a result, in Figure 7 the scattering is shown for the ratio between the angle $\phi(x_{MEMS})$, see (10), and δ,

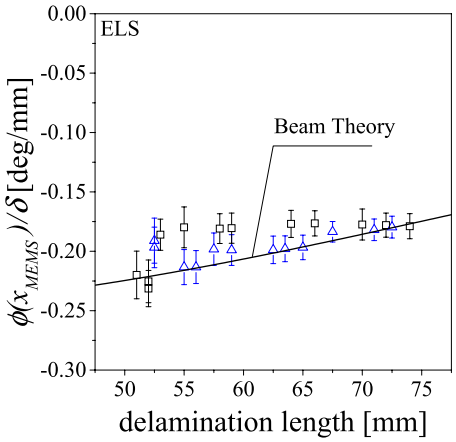

Fig. 7. ELS test: statistics of the measured inclination angle, and theoretical prediction by beam theory (different symbols correspond to different samples).

during the stationary stage of each load step, along with the corresponding prediction provided by the beam theory. The limited scattering in the experimental data is here accompanied by a very good agreement between the measured and predicted values.

The present results prove that, with this test setup, the sensor can be successfully adopted to monitor the position of the delamination tip. Nevertheless, it is worth mentioning that from (9) it emerges that the angle ϕ is rather sensitive to indeterminacy in the MEMS position x_{MEMS}; hence, part of the different experimental and theoretical trends in Figure 7 can be attributed to a slightly different placement of the sensor board over different samples, mainly due to the present setup involving the use of a back plate.

The outcomes of the present investigation, supplemented by the former ones of [21], have therefore supported the claim that composite laminates can be inexpensively monitored through inertial MEMS sensors. To get effective estimations and forecasts of the structural health, we have shown that ad-hoc analyses are required to model the real behavior of the structure; this is indeed a crucial aspect of any health monitoring strategy.

V. Conclusion

Composite laminates can fail because of the inception and subsequent growth of interlaminar decohesion. Due to complex loading conditions, such decohesion does not necessarily start at the free surface in real-life structures. So, a direct visual inspection approach cannot be adopted and health monitoring systems are required to sense (hopefully in real time) changes of the structural behavior with respect to the undamaged state, without enhancing the changes themselves.

In this paper, we have provided an experimental/theoretical investigation of the effectiveness and robustness of a MEMS-based, surface-mounted health monitoring scheme for laminates. Through standard laboratory tests, like the double-cantilever-beam (DCB) and the end-loaded-split (ELS) ones, the said effectiveness has been evaluated on the basis of the sensitivity of the sensor output to the size of the delaminated area; the robustness has been instead assessed through the repeatability of the results at varying specimen. The accelerations sensed by a commercial-off-the-shelf, three-axis MEMS accelerometer has been post-processed to obtain structural information, validated through comparison with a simultaneous measurement of the specimen compliance (which is proportional to the delamination size). To this purpose, mechanical models based on beam bending theory have been discussed for the samples featuring a pre-existing delamination, progressively growing under cycling (sinusoidally varying) loadings.

Independently of the local loading condition at the delamination tip (namely, independently of the test setup), the experimental trends, shown at increasing delamination length, have been in good agreement with those foreseen by beam bending, as already partially discussed in [21].

To avoid or, at least, reduce issues related to the scattering of the experimental outcomes, in future investigations a network of sensors, appropriately deployed over the samples or structures, will be adopted. Powering of the network and synchronization of the sensors output will be therefore investigated too.

References

[1] J. D. Achenbach, "Structural health monitoring—What is the prescription?" *Mech. Res. Commun.*, vol. 36, no. 2, pp. 137–142, 2009.

[2] S. C. Mukhopadhyay, J. G. Chase, and N. Meyendorf, "Editorial special issue on sensors systems for structural health monitoring," *IEEE Sensors J.*, vol. 9, no. 11, pp. 1319–1321, Nov. 2009.

[3] S. Gopalakrishnan, M. Ruzzene, and S. Hanagud, *Computational Techniques for Structural Health Monitoring*. London, U.K.: Springer-Verlag, 2011.

[4] S. Nemat-Nasser and M. Hori, *Micromechanics: Overall Properties of Heterogeneous Materials* (Applied Mathematics and Mechanics), vol. 37, J. D. Achenbach, B. Budiansky, H. A. Lauwerier, P. G. Saffman, L. van Wijngaarden, and J. Willis, Eds. Amsterdam, The Netherlands: North Holland, 1993.

[5] J. Reddy, *Mechanics of Laminated Composite Plates and Shells: Theory and Analysis*. Boca Raton, FL, USA: CRC Press, 2004.

[6] S. Li and G. Wang, *Introduction to Micromechanics and Nanomechanics*. Singapore: World Scientific, 2008.

[7] O. Allix, P. Ladevéze, and A. Corigliano, "Damage analysis of interlaminar fracture specimens," *Compos. Struct.*, vol. 31, no. 1, pp. 61–74, 1995.

[8] A. Corigliano, "Damage and fracture mechanics techniques for composite structures," in *Comprehensive Structural Integrity*, vol. 3, I. Milne, R. Ritchie, and B. Karihaloo, Eds. Amsterdam, The Netherlands: Elsevier, 2003, ch. 9, pp. 459–539.

[9] S. Mariani and A. Corigliano, "Impact induced composite delamination: State and parameter identification via joint and dual extended Kalman filters," *Comput. Methods Appl. Mech. Eng.*, vol. 194, no. 50, pp. 5242–5272, 2005.

[10] M. Mieloszyk, L. Skarbek, M. Krawczuk, W. Ostachowicz, and A. Zak, "Application of fibre Bragg grating sensors for structural health monitoring of an adaptive wing," *Smart Mater. Struct.*, vol. 20, no. 12, p. 125014, 2011.

[11] B. Torres, I. Paya-Zaforteza, P. A. Calderon, and J. M. Adam, "Analysis of the strain transfer in a new FBG sensor for structural health monitoring," *Eng. Struct.*, vol. 33, no. 2, pp. 539–548, 2011.

[12] A. Purekar and D. Pines, "Damage detection in thin composite laminates using piezoelectric phased sensor arrays and guided lamb wave interrogation," *J. Intell. Mater. Syst. Struct.*, vol. 21, no. 10, pp. 995–1010, 2010.

[13] A. Orlowska, P. Kolakowski, and J. Holnicki-Szulc, "Detecting delamination zones in composites by embedded electrical grid and thermographic methods," *Smart Mater. Struct.*, vol. 20, no. 10, p. 105009, 2011.

[14] S. M. Nalawade, N. Mahra, K. T. V. Grattan, and H. V. Thakur, "Delamination detection in glass composites using embedded Hi-Bi photonic crystal fiber," *Smart Mater. Struct.*, vol. 20, no. 5, p. 055023, 2011.

[15] A. Kousourakis, M. Bannister, and A. Mouritz, "Tensile and compressive properties of polymer laminates containing internal sensor cavities," *Compos. A, Appl. Sci. Manuf.*, vol. 39, no. 9, pp. 1394–1403, 2008.
[16] M. Melnykowycz and A. J. Brunner, "The performance of integrated active fiber composites in carbon fiber laminates," *Smart Mater. Struct.*, vol. 20, no. 7, p. 075007, 2011.
[17] S. Butler *et al.*, "Effect of embedded sensors on interlaminar damage in composite structures," *J. Intell. Mater. Syst. Struct.*, vol. 22, no. 16, pp. 1857–1868, 2011.
[18] H. P. Konka, M. A. Wahab, and K. Lian, "The effects of embedded piezoelectric fiber composite sensors on the structural integrity of glass-fiber-epoxy composite laminate," *Smart Mater. Struct.*, vol. 21, no. 1, p. 015016, 2012.
[19] H.-Y. Tang, C. Winkelmann, W. Lestari, and V. La Saponara, "Composite structural health monitoring through use of embedded PZT sensors," *J. Intell. Mater. Syst. Struct.*, vol. 22, no. 8, pp. 739–755, 2011.
[20] G. Pereira, C. Frias, H. Faria, O. Frazão, and A. Marques, "Study of strain-transfer of FBG sensors embedded in unidirectional composites," *Polymer Test.*, vol. 32, no. 6, pp. 1006–1010, 2013.
[21] S. Mariani, A. Corigliano, F. Caimmi, M. Bruggi, P. Bendiscioli, and M. De Fazio, "MEMS-based surface mounted health monitoring system for composite laminates," *Microelectron. J.*, vol. 44, no. 7, pp. 598–605, 2013.
[22] C. Ratcliffe, D. Heider, R. Crane, C. Krauthauser, M. K. Yoon, and J. W. Gillespie, "Investigation into the use of low cost MEMS accelerometers for vibration based damage detection," *Compos. Struct.*, vol. 82, no. 1, pp. 61–70, 2008.
[23] *Standard Test Method for Mode I Interlaminar Fracture Toughness of Unidirectional Fiber-Reinforced Polymer Matrix Composites*, Standard ASTM D-5528, 2007.
[24] A. Russell and K. Street, "The effect of matrix toughness on delamination: Static and fatigue fracture under mode II shear loading of graphite fiber composites," in *Toughened Composites ASTM STP 937*, N. Johnston, Ed. Philadelphia, PA, USA: ASTM, 1987, pp. 271–289.
[25] P. Powell, *Engineering With Fibre-Polymer Laminates*. Berlin, Germany: Springer-Verlag, 1994.
[26] D. Hull and T. Clyne, *An Introduction to Composite Materials* (Cambridge Solid State Science), 2nd ed. Cambridge, U.K.: Cambridge Univ. Press, 1996.
[27] *LIS3LV02DQ Datasheet*, STMicroelectronics, Geneva, Switzerland, 2005.
[28] S. Mariani, A. Corigliano, F. Caimmi, M. Bruggi, P. Bendiscioli, and M. De Fazio, "Health monitoring of flexible composite plates: A MEMS-based approach," in *Proc. MicroTech Conf. Expo*, Santa Clara, CA, USA, Jun. 2012, pp. 227–230.
[29] J. Williams, "Large displacement and end block effects in the 'DCB' interlaminar test in modes I and II," *J. Composite Mater.*, vol. 21, no. 4, pp. 330–347, 1987.
[30] M. Bruggi and S. Mariani, "Optimization of sensor placement to detect damage in flexible plates," *Eng. Optim.*, vol. 45, no. 6, pp. 659–676, 2013.
[31] S. Mariani, M. Bruggi, F. Caimmi, P. Bendiscioli, and M. De Fazio, "Sensor deployment over damage-containing plates: A topology optimization approach," *J. Intell. Mater. Syst. Struct.*, vol. 24, no. 9, pp. 1105–1122, 2013.